




 Cite this: *Sens. Diagn.*, 2023, 2, 1145

## Recent advances in PAMAM dendrimer-based CT contrast agents for molecular imaging and theranostics of cancer

 Tianyu Huang,<sup>†ab</sup> Gaoming Li,<sup>†a</sup> Yunqi Guo,<sup>a</sup> Guixiang Zhang,<sup>\*c</sup> Dzmitry Shchabin,<sup>d</sup> Xiangyang Shi <sup>\*a</sup> and Mingwu Shen <sup>\*a</sup>

Construction of poly(amidoamine) (PAMAM) dendrimer-based nanoplatfoms for tumor computed tomography (CT) imaging and theranostics has gained significant attention in recent years. The unique characteristics of PAMAM dendrimers such as monodispersity, highly branched interior, and 3-dimensional architecture allow them to be widely used in the field of biomedicine, especially for tumoral delivery of contrast agents. With the help of PAMAM dendrimers, traditional contrast agents easily accumulate at tumor sites, resulting in accurate diagnostics. Moreover, contrast agents and anticancer drugs can be integrated by PAMAM dendrimers to form multifunctional platforms for cancer theranostics. In this review, we summarize the recent advances in the construction of PAMAM dendrimer-based nanoplatfoms for tumor CT imaging and theranostics, including the optimization of platform design, imaging performance, and theranostics. The challenges and future development strategies for dendrimer-based nanoplatfoms towards laboratory study and practical biomedical applications are also discussed.

 Received 28th April 2023,  
 Accepted 18th August 2023

DOI: 10.1039/d3sd00101f

[rsc.li/sensors](https://rsc.li/sensors)

<sup>a</sup> State Key Laboratory for Modification of Chemical Fibers and Polymer Materials, Shanghai Engineering Research Center of Nano-Biomaterials and Regenerative Medicine, College of Biological Science and Medical Engineering, Donghua University, Shanghai 201620, China. E-mail: xshi@dhu.edu.cn, mwshen@dhu.edu.cn

<sup>b</sup> College of Chemistry and Chemical Engineering, Donghua University, Shanghai 201620, China

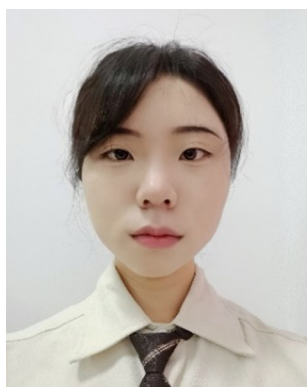
<sup>c</sup> Department of Radiology, Shanghai Fourth People's Hospital, School of Medicine, Tongji University, Shanghai 200434, China

<sup>d</sup> Institute of Biophysics and Cell Engineering of NASB, Akademicheskaya 27, 220072 Minsk, Belarus

<sup>†</sup> These authors contributed equally to this work.

## 1. Introduction

Cancer is a major global public health problem and remains one of the deadliest diseases.<sup>1</sup> The first step in cancer management is diagnosis, and early detection and treatment of cancer is the most effective way to save patients' lives. There are many different imaging modalities currently used to diagnose cancer, such as computed tomography (CT), fluorescence imaging, magnetic resonance (MR) imaging, and positron emission tomography (PET) imaging, which


**Tianyu Huang**

Tianyu Huang obtained her BS degree in Chemistry from Henan Normal University. Currently, she is a master's student at the School of Chemistry and Chemical Engineering, Donghua University, supervised by Prof. Mingwu Shen. Her current research project focuses on the preparation of nanogel-based platforms for theranostic applications.


**Gaoming Li**

Gaoming Li obtained his MS degree in 2021 from the College of Chemistry, Chemical Engineering and Biotechnology, Donghua University, under the supervision of Prof. Xiangyang Shi. Currently, he is a Ph.D. candidate in the College of Biological Science and Medical Engineering, Donghua University, supervised by Prof. Mingwu Shen. His current research project is focused on the preparation of layered double hydroxide-based functional nanohybrids for biomedical applications.



often require the use of contrast agents to improve the efficiency, resolution, and accuracy of imaging.<sup>2</sup>

CT imaging is one of the most representative imaging methods. In recent years, many studies have shown that CT imaging, as a non-invasive, economical and reproducible imaging mode, enables early diagnosis, genotype prediction, efficacy assessment and prognosis evaluation of cancer. For example, Wang *et al.* reported CT imaging features as predictors of tumor mutation burden and driver mutations in patients with early-stage lung adenocarcinoma.<sup>3</sup> Tsili *et al.* summarized studies of multidetector CT imaging in breast cancer and concluded that its advantages include increased volume coverage, reduced scan time frame, and ability of acquisition of thin slices and generation of multiplanar and three-dimensional reconstructions, and CT can provide

useful information for early and accurate detection of peritoneal metastases.<sup>4</sup> The most commonly used contrast agent for CT imaging is Omnipaque, a low-molecular-weight contrast agent with drawbacks such as high nephrotoxic concentrations, low imaging efficiency, rapid metabolism resulting in a short imaging time window, and lack of specificity.<sup>5</sup> Therefore, development of suitable contrast agents, which selectively accumulate in tumors with enhanced CT image visibility, is essential to improve the efficiency of CT imaging to reduce the side effects of contrast agents.

In recent years, the development of nanomedicine has expanded the boundaries of biomedical research, especially in the field of tumor diagnosis and treatment. Among various nanomaterials, poly(amidoamine) (PAMAM) dendrimers are a class of synthetic, highly branched and monodisperse nanoparticles that have gained increasing attention as nanoplatforms for tumor diagnosis and treatment.<sup>6</sup> PAMAM dendrimers have a well-defined structure and surface functional groups, allowing for the incorporation of various imaging and therapeutic agents as well as targeting moieties to achieve specific functions.<sup>7</sup> This makes them ideal candidates for the development of nanoprobcs for tumor CT imaging. For example, functionalization of PAMAM dendrimers with a variety of ligands can greatly increase their targeting specificity and improve their performance of specific imaging. Meanwhile, the periphery of the PAMAM dendrimers can also be grafted with many other imaging elements for dual-modality or multimodality imaging.<sup>8</sup> Importantly, appropriate modifications to the surface of the dendrimers can improve their biocompatibility.<sup>9</sup> In addition, the size of the dendrimers can be adjusted through formation of dendrimer nanoclusters, dendrimer nanogels or core-shell tecto dendrimers (CSTDs) as required to meet the timing of imaging needs with controlled excretion behaviour.<sup>10–12</sup>



**Guixiang Zhang**

*Guixiang Zhang, MD, Chief Physician, professor and doctoral supervisor at Shanghai Fourth People's Hospital, School of Medicine, Tongji University, obtained his PhD in clinical medical imaging in 1993, received a diploma as a foreign attending physician from the School of Medicine at the University of Lyon in France in 1993 and was employed as a physician at the Department of Radiology of Nancy Neurological*

*Hospital in France in 1995. Dr. Zhang has rich experience in clinical medical imaging diagnosis, and has published over 100 SCI-indexed peer-reviewed journal articles.*



**Xiangyang Shi**

*Xiangyang Shi obtained his PhD degree in 1998 from the Chinese Academy of Sciences. From 2002 to 2008, he was appointed as a research fellow, research associate II, research investigator, and research assistant professor in the Medical School of University of Michigan, Ann Arbor. In September 2008, he joined Donghua University as a full professor. He has published 496 peer-reviewed SCI-indexed journal articles with an h-index*

*of 86. His current research interests are focused on the development of organic/inorganic hybrid nanoplatforms and dendrimeric nanoparticles for sensing, imaging, and theranostic applications, in particular for precision cancer imaging and therapy.*



**Mingwu Shen**

*Mingwu Shen received her PhD degree in 2001 from Tsinghua University. Afterwards, she went to the University of Michigan, Ann Arbor, as a visiting scholar and a research area specialist intermediate. She joined Donghua University as an associate professor in 2008, and since 2017, she has been appointed as a full professor of Biomedical Engineering at Donghua University. She has published more than 210 SCI-*

*indexed peer-reviewed journal articles with an h-index of 60. Prof. Shen's current research interests include organic/inorganic hybrid nanoparticle-based platforms for medical imaging and therapy applications.*



With the development of tumor biology and nanomedicine, our group and other researchers have developed a series of PAMAM dendrimer-based nanoplatfoms for CT imaging over the past 15 years. In recent years, in order to develop ideal CT contrast agents, researchers have explored in detail to improve the biocompatibility, targeting specificity and efficiency, and multifunctionality of PAMAM dendrimer-based nanoplatfoms (Table 1). Therefore, in this review, we attempt to summarize the recent advances in the use of PAMAM dendrimer-based nanoplatfoms for CT imaging. Since Qiao *et al.* have summarized the dendrimer-based nanoplatfoms for molecular imaging up to 2015, this review mostly summarizes the progress from 2016 to the present. It should be noted that this is not a comprehensive review to cover all aspects of PAMAM dendrimer-based nanoplatfoms for CT imaging, but rather to discuss some of the key developments in the synthesis and functionalization of these nanoplatfoms for CT imaging applications, including single-mode/dual-mode imaging and theranostic applications (Fig. 1). Finally, the challenges and outlook of PAMAM dendrimer-based nanoplatfoms for CT imaging and theranostics are also briefly discussed.

## 2. Structural design and optimization of PAMAM dendrimer-based nanoplatfoms as CT contrast agents

### 2.1 PAMAM dendrimers as scaffolds for iodinated CT contrast agents

The most commonly used CT contrast agents in clinical practice are small-molecule iodinated contrast agents (*e.g.* Omnipaque), but these contrast agents have disadvantages such as nephrotoxicity, fast metabolism, and low specificity.<sup>13</sup> As a nano-sized polymer, PAMAM dendrimer is an ideally suitable scaffold to load iodinated contrast agents, thus overcoming many of the drawbacks of iodinated contrast agents and being adapted for CT imaging of various biological systems.<sup>14</sup> Many studies have reported the use of dendritic polymers as scaffolds to load iodinated CT contrast agents. Previously, our group has shown that diatrizoic acid (DTA), a kind of iodine(I)-based CT contrast agent with carboxyl groups, can be successfully modified on the surface of dendrimers *via* a 1-ethyl-3-(3-(dimethylamino)propyl)-carbodiimide hydrochloride (EDC)

**Table 1** Summary of representative PAMAM dendrimer-based nanoplatfoms for CT imaging applications from 2016 to the present

| Application   | Nanoplatfoms   | Dendrimer generation      | Contrast agents                                | Delivery strategies              | Imaging         | Ref. |
|---|--|---------------------------|--|----------------------------------|-----------------|------|
| Single-mode imaging   | D1–D4  | G1–G4                     | Tetraiodobenzene derivatives                   | Polyethylene glycol (PEG)        | CT              | 18   |
|   | PEG-citrate dendrimer-G2-iohexol   | G2                        | Iohexol  | PEG                              | CT              | 19   |
|   | [(Au <sup>0</sup> ) <sub>300</sub> -G5-NHAc-mPEG] DENPs                              | G5                        | Au NPs   | PEG                              | CT              | 10   |
|   | (Au <sup>0</sup> ) <sub>100</sub> -G5-NHAc-CBAA <sub>80</sub>                        | G5                        | Au NPs   | Carboxybetaine acrylamide (CBAA) | CT              | 20   |
| Dual-mode imaging   | [(Au <sup>0</sup> ) <sub>120</sub> -G5-NHAc-DTA-(PEG-FA)-mPEG] DSNs                  | G5                        | Au NPs, diatrizoic acid (DTA)                  | FA                               | CT              | 17   |
|   | Au(P5-LA) DENPs  | G5                        | Au NPs   | Lactobionic acid (LA)            | CT              | 21   |
|   | RGD-Au-Mn DENPs  | G2                        | Au NPs, Mn                                     | Arginine-glycine-aspartic (RGD)  | CT/MR           | 22   |
|   | RGD-Gd-Au DEN-PS   | G5                        | Au NPs, Gd                                     | 1,3-Propanesultone (1,3-PS), RGD | CT/MR           | 23   |
|   | G5-Au NP-Gd-trastuzumab  | G5                        | Au NPs, Gd                                     | Trastuzumab                      | CT/MR           | 24   |
|   | Gd-Au DENPs-FA   | G5                        | Au NPs, Gd                                     | FA                               | CT/MR           | 25   |
|   | (Au <sup>0</sup> ) <sub>100</sub> -G5-NH <sub>2</sub> -FI-DOTA(Mn)-HA                | G5                        | Au NPs, Mn                                     | Hyaluronic acid (HA)             | CT/MR           | 26   |
|   | RGD-Gd@Au CSTDs-PS   | G3, G5                    | Au NPs, Gd                                     | 1,3-PS, RGD                      | CT/MR           | 11   |
|   | RGD-Gd@Au-DNGs-PS  | G3                        | Au NPs, Gd                                     | 1,3-PS, RGD                      | CT/MR           | 27   |
|   | MA-laden Fe <sub>3</sub> O <sub>4</sub> /Au DSNFs                                    | G5                        | Au nanoflowers, Fe <sub>3</sub> O <sub>4</sub> | Macrophages                      | CT/MR           | 28   |
|   | (Au <sup>0</sup> ) <sub>25</sub> -G5-NHAc-(PEG) <sub>14</sub> -(Fluo-4) <sub>2</sub> | G5                        | Au NPs, Fluo-4                                 | PEG                              | CT/fluorescence | 29   |
|   | (Au <sup>0</sup> ) <sub>6</sub> -G2-DTPA ( <sup>99m</sup> Tc)-PEG-FA                 | G2                        | Au NPs, <sup>99m</sup> Tc                      | FA                               | SPECT/CT        | 30   |
|   | (Au <sup>0</sup> ) <sub>6</sub> -G2-NOTA ( <sup>99m</sup> Tc)-PEG-RGD                | G2                        | Au NPs, <sup>99m</sup> Tc                      | RGD                              | SPECT/CT        | 31   |
| <sup>99m</sup> Tc-duramycin-Au DENPs                                    | G5   | Au NPs, <sup>99m</sup> Tc | Duramycin                                      | SPECT/CT                         | 32              |      |
| (Au <sup>0</sup> ) <sub>6</sub> -G2- <sup>99m</sup> Tc-DTPA-(PEG-FC131) | G2   | Au NPs, <sup>99m</sup> Tc | FC131 peptide                                  | SPECT/CT                         | 33              |      |
| Theranostics  | RGD-Au DSNs/siRNA  | G3                        | Au nanostars                                   | RGD                              | CT, thermal     | 34   |
|   | Fe <sub>3</sub> O <sub>4</sub> /Au DSNFs   | G5                        | Au nanoflowers, Fe <sub>3</sub> O <sub>4</sub> | —                                | CT/MR/PA        | 35   |
|   | Apt-PEG-Au-PAMAM-CUR   | G5                        | Au NPs   | MUC-1 aptamer                    | CT              | 36   |
|   | Au-G5-F-D  | G5                        | Au NPs   | FA                               | CT              | 37   |
|   | Gd-Au DENPs-Nit  | G5                        | Au NPs, Gd                                     | 2-Nitroimidazole                 | CT/MR           | 38   |
|   | <sup>111</sup> In-Asp-PAMAM-Micelles   | G3                        | Ca   | Aspartic acid (Asp)              | SPECT/CT        | 39   |
|   | DRC  | G5                        | Au NPs, Gd                                     | 1,3-PS                           | CT/MR           | 40   |
|   | Au NR@PAMAM-GX1/FAM172A  | G3                        | Au nanorods                                    | GX1 peptide                      | CT              | 41   |
|   | Au DENPs@Macs  | G5                        | Au NPs   | Macrophage                       | CT              | 42   |
|   | DG- <sup>68</sup> Ga-Au DENPs/CpG  | G5                        | Au NPs, <sup>68</sup> Ga                       | Glucose                          | PET/CT          | 43   |
|   | Col-I@G5AuNP   | G5                        | Au NPs   | Collagen I                       | CT              | 44   |





Fig. 1 Schematic design of nanostructures of PAMAM dendrimer-based nanoplatforms as CT contrast agents.

coupling reaction.<sup>15–17</sup> In addition, You *et al.* developed new iodinated dendritic CT contrast agents for the first time using tetraiodophthalic anhydride (TIPN) as potent radiopaque molecules (Fig. 2) and tested the feasibility of this approach using amine-terminated PAMAM dendrimers.<sup>18</sup> The developed agent exhibited high performance with highly desirable contrast enhancement, osmolarity values and blood half-life for tumor

diagnosis. Likewise, it has no significant toxicity, showing no animal damaging properties *in vivo*.

## 2.2 PAMAM dendrimers as scaffold for gold CT contrast agents

Gold (Au) nanoparticles (NPs) possess unique physicochemical properties and various biological activities, which have been

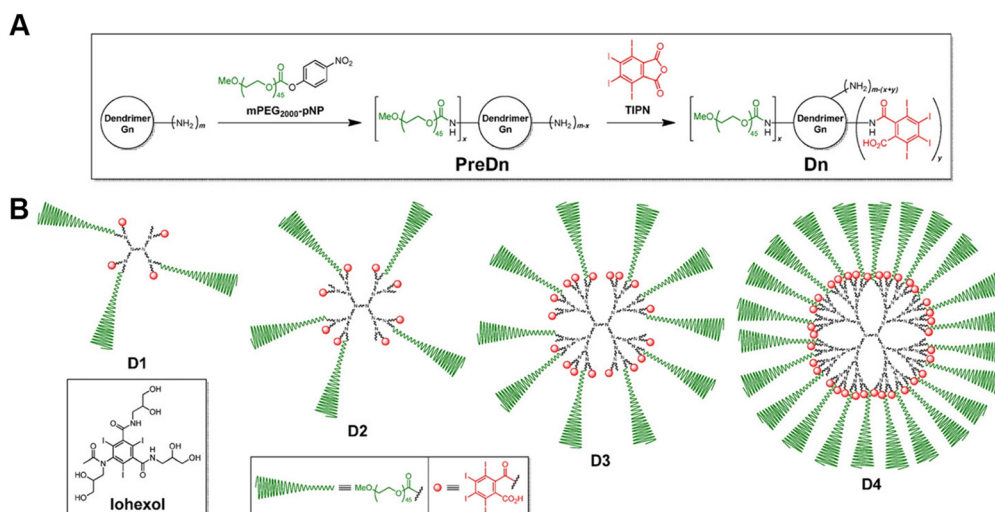


Fig. 2 (A) General synthetic scheme and (B) schematic illustrations of the dendritic CT contrast agents, D1–D4. Iohexol was used as a rapidly excreted small-molecule control in the *in vivo* experiments. D1–D4 were prepared in two steps, starting from an amine-terminated  $n$ th generation ( $G_n$ ) dendrimer ( $m = 2^{n+2}$ , for PAMAM dendrimers used herein), via the stoichiometrically controlled sequential attachment of polyethylene glycol (PEG) monomethyl ether (mPEG) and TIP units. Each compound consists of a central dendrimer (black) as a scaffold, biocompatible mPEG units (green) for stealth effects, and TIPN moieties (red) as radiopaque agents. Reproduced with permission.<sup>18</sup> Copyright 2016, Elsevier.



widely studied and applied in the biomedical field. In recent years, our group has conducted a series of studies on the use of dendrimer-entrapped Au NPs (Au DENPs) for CT imaging. Compared with traditional I-based CT contrast agents, Au DENPs can not only overcome the shortcomings of traditional contrast agents but also have the following advantages: (1) Au has a higher atomic number than I, thus having a better X-ray attenuation performance and better contrast than I-based CT agents; (2) nano-sized Au DENPs can prolong the blood circulation time for enhanced tumor CT imaging applications through an enhanced permeability and retention (EPR) effect; (3) the peripheral amine groups of dendrimers can be further functionalized to make them biocompatible, target specific and multifunctional.<sup>8,45,46</sup> Unlike the nanoarchitectures of Au DENPs, PAMAM dendrimer-stabilized Au NPs (Fig. 3A), Au nanostars (Fig. 3B), Au nanoflowers (Fig. 3C), and Au nanorods (Fig. 3D) have also been developed for CT imaging.<sup>17,34,35,41</sup> In addition to dendrimer-based CT imaging nanoplateforms loaded with iodinated agents or Au NPs, dendrimer-based nanoplateforms integrating both Au and I imaging components have also been reported.<sup>15,17</sup>

Due to the cavity inside the dendrimer and the easily functionalized surface amine groups at the dendrimer periphery, dendrimers are able to physically wrap or covalently connect iron oxide ( $\text{Fe}_3\text{O}_4$ ) NPs, manganese ions ( $\text{Mn}^{2+}$ ), gadolinium ions ( $\text{Gd}^{3+}$ ), fluorescent molecules, radioactive elements, *etc.* after entrapping Au NPs for dual-modal or multimodal imaging, such as CT/MR, CT/fluorescence imaging, SPECT/CT, *etc.*<sup>22,23,29</sup> Furthermore, the dendrimer-based nanocomplexes can be loaded with chemotherapeutic drugs or genetic drugs inside or on the surface to build up theranostic nanoplateforms for monitoring the tumor treatment process and thus better studying the tumor treatment mechanism.<sup>34,35,37</sup>

### 2.3 Strategies to improve the tumor delivery of PAMAM dendrimer-based nanoplateforms

Compared to small-molecule contrast or therapeutic agents, nanoagents are able to passively target tumors through the EPR effect, thus enhancing their diagnostic or therapeutic outcomes. However, nanoagents after intravenous injection have to go through a series of key steps, including blood circulation (C), accumulation to the tumor (A), penetration (P), internalization (I), and drug release (R). These five steps are referred to as the CAPIR cascade. Only when the CAPIR

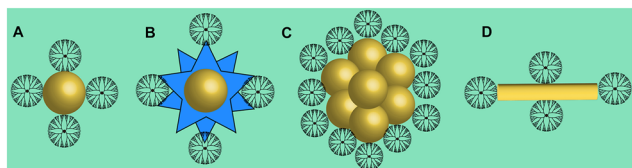


**Fig. 3** Schematic structures of PAMAM dendrimer-stabilized (A) Au NPs, (B) Au nanostars, (C) Au nanoflowers, and (D) Au nanorods.

process is successfully implemented can a therapeutic effect be guaranteed.<sup>47</sup> For PAMAM dendrimer-based nanoplateforms used in CT imaging, prolonging the blood circulation time and increasing their accumulation at the tumor site can effectively improve the imaging quality and sensitivity.

In recent years, a series of structural designs and surface modifications of dendrimer-based nanoplateforms, such as the construction of CSTDs and dendrimer nanogels, surface PEGylation, and zwitterion and targeting ligand modifications, have been carried out to amplify the EPR-based tumor targeting effect. The design and surface modification of dendrimers can prolong the blood circulation time, enhance the passive tumor targeting ability or render the nanoplateforms with active targeting specificity to tumors. These effects have been demonstrated in various tumor models.<sup>11,12</sup> In an early attempt, PEG-modified generation 5 (G5) dendrimers were used as templates to synthesize Au DENPs, followed by acetylation of the remaining dendrimer terminal amines to generate PEGylated Au DENPs. The results of *in vivo* experiments show that the formed PEGylated Au DENPs have good biocompatibility and can enhance CT imaging.<sup>10</sup> Subsequently, literature reports have shown that zwitterion-modified nanomaterials have good antifouling properties, prolonged blood circulation time, and enhanced tumor penetration and retention. The reason for this is that each ion pair of positive and negative groups can immobilize a large number of water molecules around and form a protective layer of water on the nanomaterial surface, thus shielding the hydrophobic interactions between contaminants and the nanomaterial surface. For example, we reported the synthesis and characterization of antifouling zwitterion carboxybetaine acrylamide (CBAA)-modified Au DENPs (Fig. 4A and B). Protein resistance assay, macrophage cellular uptake, and pharmacokinetic studies showed that the zwitterion CBAA modification renders the Au DENPs with much better antifouling properties than the PEG-modified counterpart, and increasing the amount of its modification can enhance the antifouling effect of the material. With good cytocompatibility and high X-ray attenuation intensity, the CBAA-modified Au DENPs enable enhanced tumor CT imaging (Fig. 4C and D).

It has been found that active targeting by modifying targeting ligands on the surface of nanomaterials through receptor–ligand recognition enables nanomaterials to better reach the lesion site. Our group explored the antifouling properties of G5 dendrimers partially modified with CBAA, 2-methacryloyloxyethyl phosphorylcholine (MPC), and 1,3-propanesultone (1,3-PS), respectively, to different degrees,<sup>23</sup> and showed that 1,3-PS-modified dendrimers had the best antifouling properties and could significantly prolong the blood circulation time (Fig. 5A). With the optimized zwitterion type, we then prepared Gd(III)-loaded Au DENPs modified with 1,3-PS and arginine–glycine–aspartic (RGD) peptide for targeted dual-mode CT/MR imaging of a lung cancer metastasis model (Fig. 5B–E). In addition, the use of cancer cell membrane homologous targeting effect<sup>48,49</sup> and macrophage- or macrophage membrane-based tumor homing effect<sup>50,51</sup> to





**Fig. 4** (A) Schematic illustration of the synthesis of CBAA- or PEG-modified Au DENPs and (B) the good antifouling properties of CBAA-modified Au DENPs in blood vessels for imaging applications. (C) CT images and (D) CT values of the U87MG tumor in nude mice at different time points post intravenous injection of  $\{(Au^0)_{100}\text{-G5-NHAc-CBAA}_{20}\}$  (1),  $\{(Au^0)_{100}\text{-G5-NHAc-CBAA}_{80}\}$  (2) or  $\{(Au^0)_{100}\text{-G5-NHAc-mPEG}_{20}\}$  (3) ( $[Au] = 0.1 \text{ M}$ , in  $150 \mu\text{L}$  saline,  $n = 3$ ). Reproduced with permission.<sup>20</sup> Copyright 2017, The Royal Society of Chemistry.

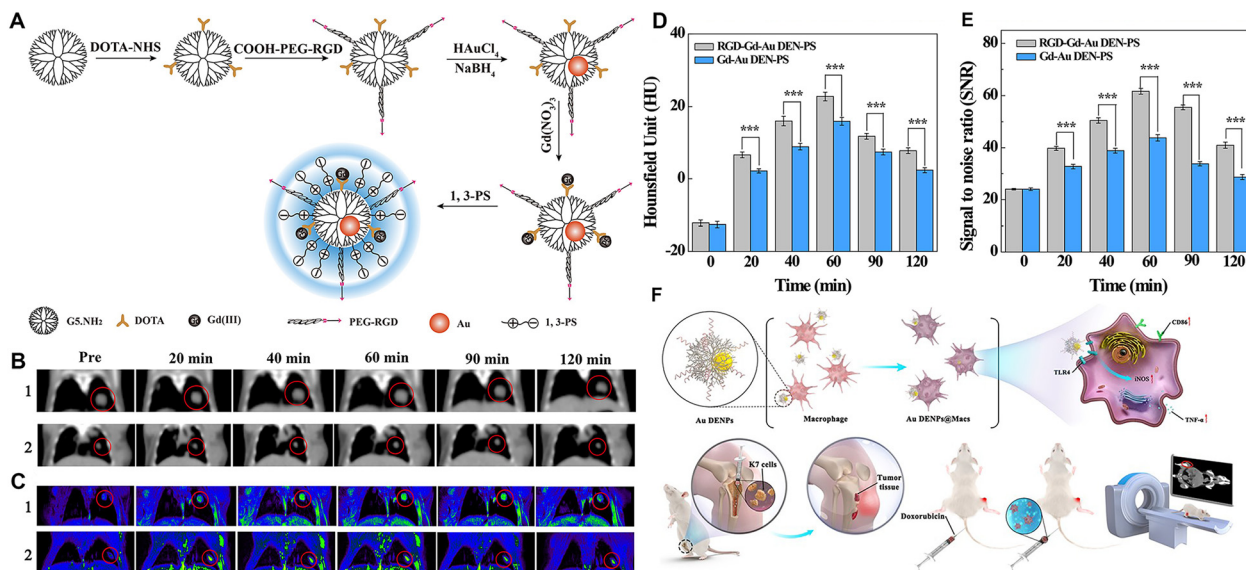


**Fig. 5** (A) Synthesis of RGD-Gd-Au DEN-PS. (B) *In vivo* CT images, (C)  $T_1$ -weighted MR images, (D) CT values, and (E) MR signal-to-noise ratio (SNR) of B16 lung cancer metastasis model at different time points post-intravenous injection of RGD-Gd-Au DEN-PS (1) or Gd-Au DEN-PS (2). The red circles indicate the tumor area. Reproduced with permission.<sup>23</sup> Copyright 2019, American Chemical Society. (F) Schematic diagram of the preparation of the Au DENPs@Macs and their application for CT imaging and combined chemotherapy/cell therapy of osteosarcoma. Reproduced with permission.<sup>42</sup> Copyright 2021, Elsevier.

render nanomaterials with enhanced tumor delivery has received increasing attention. In a recent work, Yin *et al.* developed Au DENP-engineered macrophages (Au DENPs@Macs) as a theranostic platform for CT imaging-guided cooperative immune cell therapy and chemotherapy of osteosarcoma. In this work, Au DENPs were used to activate macrophages into the anti-tumorigenic M1-like phenotype with increased expression of CD86, inducible type of nitric oxide synthase, and tumor necrosis factor- $\alpha$ . The formed Au DENPs@Macs had cytostatic/pro-apoptotic effects against an

osteosarcoma tumor model while simultaneously achieving the tumor CT imaging (Fig. 5F).<sup>42</sup>

### 3. PAMAM dendrimer-based nanoplatforms for CT imaging and theranostic applications

As above, we summarized the composition and structure of dendrimer-based nanoplatforms for CT imaging and



therapeutic integration and strategies to improve tumor delivery efficiency, in which some of the advances have been described. In this section, we mainly present some representative research advances.

### 3.1 PAMAM dendrimer-based nanoplatforms for single-mode CT imaging

PAMAM dendrimer-based nanoplatforms for CT imaging are mainly based on the entrapment of Au NPs within the dendrimer interior or the surface periphery attachment with I-containing contrast agents. Recently, our group developed an innovative nanoprobe based on G5 dendrimer-stabilized Au NPs (Au DSNs) linked with folic acid (FA) as a targeting ligand and diatrizoic acid (DTA) as a 2nd CT imaging element for enhanced specific tumor CT imaging (Fig. 6).<sup>17</sup> The formed novel materials of Au DSNs–DTA–FA have the desired colloidal stability, good cytocompatibility and hemocompatibility, and can be specifically taken up *in vitro* by cancer cells overexpressing FA receptors. The Au DSNs–DTA–FA containing both Au and I dual radiodense elements exhibit enhanced CT imaging performance, much higher than that of the single-radiodense elemental material solely based on Au or I. With the demonstrated FA-rendered specific targeting, the developed Au DSNs–DTA–FA can be employed as a highly efficient nanoprobe for targeted enhanced CT imaging of a subcutaneous tumor model.

### 3.2 PAMAM dendrimer-based nanoplatforms for dual-mode or multimode imaging

The construction of dual-modal or multimodal PAMAM dendrimer-based nanoplatforms can overcome the drawbacks of a single imaging modality while providing more accurate imaging information. In our recent work, we reported an RGD-modified low-generation dendrimer-based nanoprobe chelating Mn ions and entrapping Au NPs for CT/MR dual-modality imaging of an orthotopic brain glioma mouse model.<sup>22</sup> In this work, the G2 PAMAM dendrimers were first

modified with 1,4,7-triacyclononane-1,4,7-triacetic acid (NOTA) and the targeting ligand of RGD peptide *via* a spacer of PEG. Au DENPs were then synthesized using the functionalized G2 dendrimers as templates, followed by chelation with Mn(II) (Fig. 7A). The developed RGD–Au–Mn DENPs have good colloidal stability, higher  $r_1$  relaxivity ( $9.88 \text{ mM}^{-1} \text{ s}^{-1}$ ) than the commercial MR contrast agent Magnevist ( $4.3 \text{ mM}^{-1} \text{ s}^{-1}$ ) based on the molar concentration of the paramagnetic metal (Mn or Gd), better CT imaging performance than I-based CT contrast agents, good cytocompatibility, and targeting specificity to cancer cells expressing  $\alpha_v\beta_3$  integrin. Results show that the RGD–Au–Mn DENPs could cross the blood–brain barrier and target glioma, thus enabling targeted CT/MR dual-modality imaging (Fig. 7B–E). Moreover, we also developed RGD-modified and  $^{99\text{m}}\text{Tc}$ -labeled multifunctional Au DENPs for SPECT/CT imaging. The prepared nanocomplexes with an Au core size of 1.9 nm display good colloidal stability and can be used for targeted SPECT/CT dual-mode imaging of a subcutaneous tumor model *in vivo* (Fig. 7F).<sup>31</sup> In addition, Chen *et al.* synthesized Au DENPs functionalized with gadolinium, cyanine dye (Cy5.5), and FA for targeted CT/MR/optical trimodal imaging.<sup>52</sup> In this study, Cy5.5 was conjugated to the DOTA-modified G5 dendrimer surface *via* the EDC coupling reaction. Then, the FA moieties were modified on the dendrimer surface to enable the particles to bind to the folate receptors overexpressed on cancer cells *via* ligand–receptor interaction (Fig. 7G). *In vivo* experimental results demonstrate that the synthesized Cy5.5–Gd–Au DENP–FA NPs are capable of achieving trimodal imaging in a non-small-cell lung cancer model (Fig. 7H–M).

### 3.3 PAMAM dendrimer-based nanoplatforms for theranostics

PAMAM dendrimer-based nanoplatforms can also be loaded with both therapeutic and CT contrast imaging agents for cancer theranostics, which is vital for precision cancer nanomedicine.<sup>53–55</sup> In this context, our group reported a theranostic nanoplatform for CT imaging, thermal imaging, photothermal therapy (PTT), and gene therapy of tumors. The nanoplatform was synthesized using RGD peptide-modified G3 PAMAM dendrimers to stabilize Au nanostars (Au DSNs), which were used as a gene delivery vector to complex small interfering RNA (siRNA). The results show that the RGD-targeted Au DSNs are able to compact vascular endothelial growth factor siRNA and specifically deliver siRNA to cancer cells overexpressing  $\alpha_v\beta_3$  integrin. Under near-infrared laser irradiation, the viability of cancer cells is only 20.2% after incubation with the RGD–Au DSNs/siRNA polyplexes, which is much lower than that of cells after single PTT or gene therapy treatment. Moreover, *in vivo* results show that the RGD–Au DSNs/siRNA nanocomplexes enable tumor CT imaging, thermal imaging, PTT, and gene therapy of a subcutaneous tumor model.<sup>34</sup>

Cancer cells interact with fibroblasts, immune cells and endothelial cells in their surrounding stroma to form a very



Fig. 6 Schematic presentation of the preparation of Au DSNs–DTA–FA for targeted enhanced CT imaging of tumors. Reproduced with permission.<sup>17</sup> Copyright 2020, American Chemical Society.



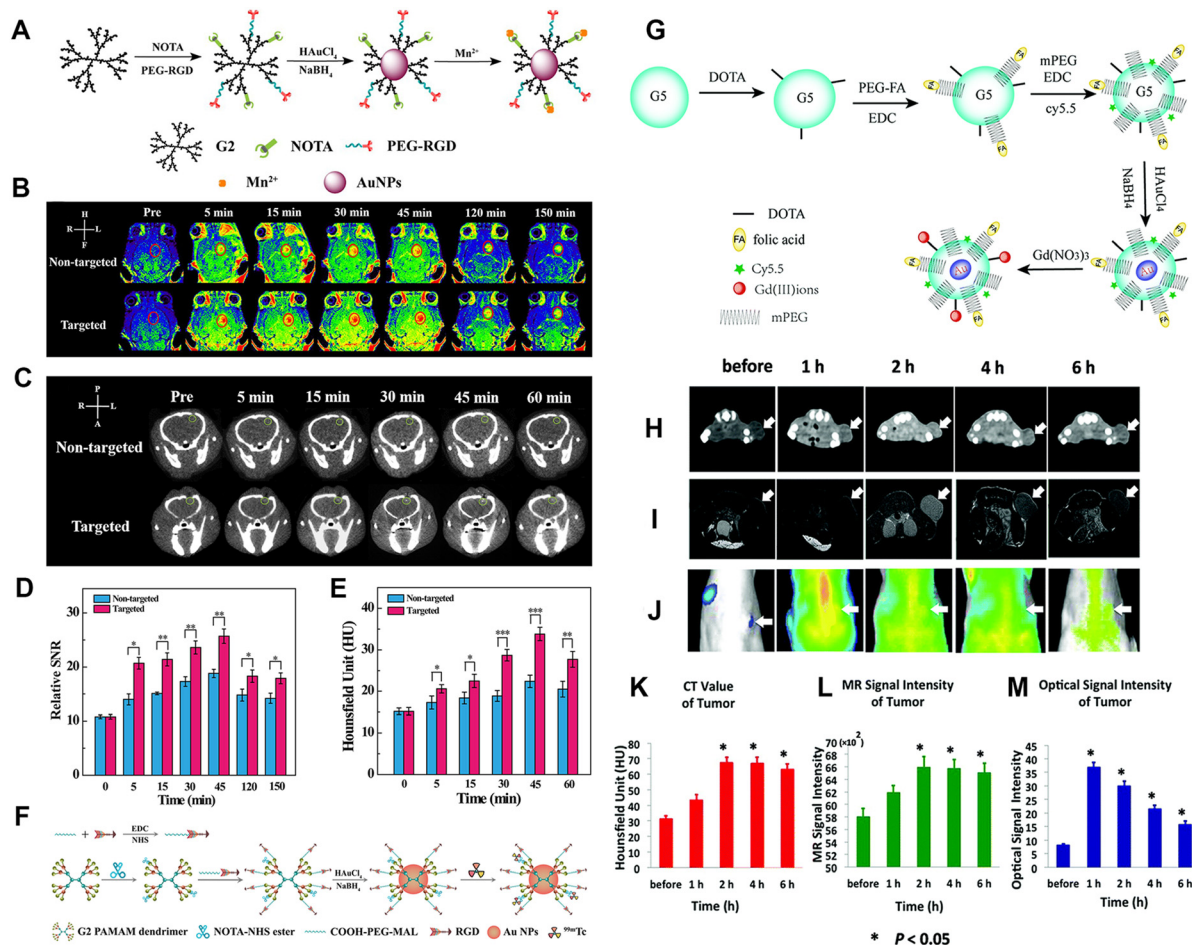


**Fig. 7** (A) Schematic diagram of the synthesis of RGD-Au-Mn DENPs. (B) The  $T_1$ -weighted MR images and the (D) MR SNR of the C6 orthotopic glioma tumor before and after the non-targeted Au-Mn or RGD-Au-Mn DENPs ( $Mn = 400$  mg,  $[Au] = 0.05$  M, in 150 mL PBS for each mouse) were intravenously injected. The red circle indicates the tumor region. (C) The CT images and (E) quantitative CT values of the C6 orthotopic glioma tumor before and after the non-targeted or RGD-targeted DENPs ( $Mn = 400$  mg,  $[Au] = 0.05$  M, in 150 mL PBS for each mouse) were intravenously injected. The green circle denotes the tumor area. Reproduced with permission.<sup>22</sup> Copyright 2019, The Royal Society of Chemistry. (F) Schematic illustration of the preparation of  $\{(Au^0)_6$ -G2-NOTA ( $^{99m}Tc$ )-PEG-RGD $\}$  DENPs. Reproduced with permission.<sup>31</sup> Copyright 2017, The Royal Society of Chemistry. (G) Synthesis of the Cy5.5-Gd-DENP-FA probe. *In vivo* CT images (H),  $T_1$ -weighted MR images (I), and optical images (J) of the xenograft NCI-H460 tumors. (K), (L), and (M) show the quantitative CT values and MR or optical signal intensities of the tumors before and after the intravenous administration of the nanoprobe, respectively. The white arrows indicate the tumor region. Reproduced with permission.<sup>52</sup> Copyright 2016, the Royal Society of Chemistry.

complex tumor microenvironment (TME), including an unusually complex and dense extracellular matrix (ECM), microvasculature and other physical factors (such as low pH, hypoxia, high hydrogen peroxide, *etc.*), which is beneficial for early tumorigenesis, development, invasion and metastasis.<sup>56–58</sup> However, the complex TME also inspires the development of various strategies for tumor diagnosis and treatment. For example, the efficacy of radiation therapy (RT) is often limited by hypoxia inside most solid tumors. In this context, we developed hypoxia-targeted Au DENPs complexed with Gd(III) (Gd-Au DENPs-Nit) for dual-mode CT/MR imaging and sensitized RT of hypoxic tumors (Fig. 8A). In this work, G5 dendrimers were partially conjugated with Gd(III) chelator, entrapped with Au NPs, and conjugated with hypoxia targeting agent nitroimidazole *via* a PEG spacer, followed by chelation of Gd(III). The formed Gd-Au DENPs-Nit

nanohybrids with an Au core size of 3.2 nm exhibit an excellent X-ray attenuation effect, acceptable  $r_1$  relaxivity ( $1.32$   $mM^{-1} s^{-1}$ ), and enhanced cellular uptake in hypoxic cancer cells, thus enabling efficient dual-mode CT/MR imaging of tumor hypoxia (Fig. 8B–G). Likewise, due to the Compton effect of Au element, the Gd-Au DENPs-Nit NPs are able to act as an effective nanosensitizer to enhance the RT efficiency of hypoxic tumors through enhancing the intracellular ROS production, enhancing DNA damage and preventing DNA repair.<sup>38</sup>

Immunotherapy, as a novel cancer treatment modality, has shown great therapeutic promise in clinical practice. Among the complex and diverse defense mechanisms of the immune system, T-cell-mediated immunity is particularly important in shaping a positive immune response against cancer cells as T cells are the main guarantors of tumor







**Fig. 8** (A) Schematic illustration of the application of Gd-Au DENPs-Nit for dual-mode CT/MR imaging and sensitized RT of tumors. The Gd-Au DENPs-Nit were tail vein injected, accumulated at the tumor site, and endocytosed by the cells for sensitized RT of tumors. (B) CT images and (C) CT values of Omnipaque (1) and Gd-Au DENPs-Nit (2) at different Au or I concentrations. (D)  $T_1$ -weighted MR images (1) and pseudocolor MR images (2) of the Gd-Au DENPs-Nit at different Gd concentrations. (E) Linear fitting of  $1/T_1$  versus Gd concentration of the Gd-Au DENPs-Nit. (F) CT values of xenografted CNE-1H tumor before and at different time points post intravenous injection of the Gd-Au DENPs or Gd-Au DENPs-Nit ( $[Au] = 100 \times 10^{-3} \text{ M}$ ). (G) Quantitative MR SNR analysis of the xenografted CNE-1H tumors before and at different time points post intravenous injection of the Gd-Au DENPs or Gd-Au DENPs-Nit ( $[Gd] = 10 \times 10^{-3} \text{ M}$ ). Reproduced with permission.<sup>38</sup> Copyright 2020, Wiley-VCH.

surveillance and cytotoxic killing.<sup>29</sup> The negative regulator of programmed cell death 1 (PD-1), also known as immune checkpoint protein, has long been known to block the cancer cell killing effect of T cells since PD-1 can bind to protein ligand 1 (PD-L1), which is abnormally expressed in several cancer cell types.<sup>59</sup> This would result in tumor escape from the immune surveillance system, suppression of the immune response and poor outcome of immunotherapy.<sup>60</sup> Blocking the PD-1 pathway is therefore a possible strategy to reverse the dysfunctional state of destructive T cells and revive their immune activity. In a very recent work, we reported a 1,3-PS-

grafted zwitterionic Au DENP platform chelated with Gd(III) (denoted as Gd-Au DENP-PS) for immune checkpoint modulation (Fig. 9A).<sup>40</sup> The developed Gd-Au DENP-PS with good stability, antifouling property, biocompatibility, and dual-mode CT/MR imaging capability enables efficient packaging and serum-enhanced delivery of PD-1 siRNA to mediate PD-1 gene silencing in T cells *in vitro* as well as *in vivo* in a melanoma-bearing mouse model. The dendrimer nanocomplexes or T-cell-loaded nanocomplexes enabled suppression of tumor growth through the generation of significant effector CD8<sup>+</sup> and CD4<sup>+</sup> T cells. The tumor



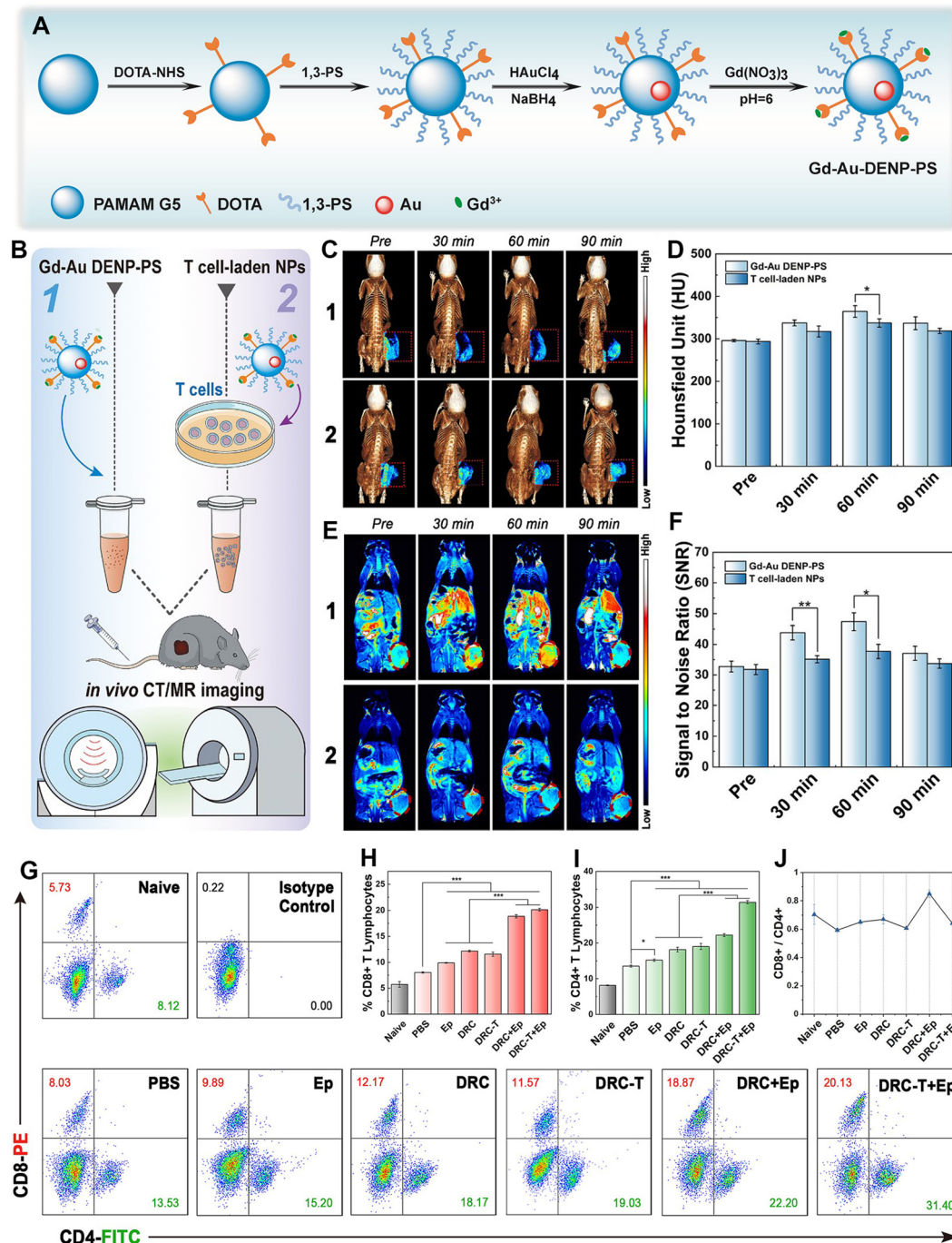
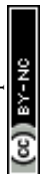


**Fig. 9** (A) Schematic illustration of the synthesis of Gd-Au DENPs-PS. (B) Schematic illustration of the *in vivo* CT/MR imaging of tumors. (C) *In vivo* 3D reconstructed micro-CT images (with pseudocolor image of the tumor site, indicated with a red dotted square) and (D) corresponding HU values. (E) *In vivo* T<sub>1</sub>-weighted pseudocolor MR images (tumor is indicated with a red dotted ellipse) and (F) corresponding tumor SNR of B16 tumor-bearing mice at different time points post intravenous injection of Gd-Au DENP-PS or T cell-laden NPs ([Au] = 25 × 10<sup>-3</sup> M in 100 μL PBS for each mouse). (G) Dot plots of CD4<sup>+</sup>/CD8<sup>+</sup> T cells, (H) CD8<sup>+</sup> T cell proportion, (I) CD4<sup>+</sup> T cell proportion, and (J) CD8<sup>+</sup>/CD4<sup>+</sup> ratio. Reproduced with permission.<sup>40</sup> Copyright 2021, Wiley-VCH.

immunotherapeutic potency can be further enhanced by combination with an indoleamine 2,3-dioxygenase inhibitor (Fig. 9B–J). In addition, our group also developed a nanoplatform based on glucose-modified Au DENPs labeled with the radionuclide <sup>68</sup>Ga and incorporated with cytosine-guanine (CpG) oligonucleotide for PET/CT dual-mode

imaging and immunotherapy of tumors. Each G5 dendrimer was first modified with 8.2 DOTA and 7.3 PEG with the other end functionalized with 2-amino-2-deoxy-D-glucose (DG). Then the functionalized dendrimers were used as templates to entrap Au NPs and then radiolabeled with <sup>68</sup>Ga through the DOTA chelation. The synthesized DG-Au DENPs were able



to target tumor cells overexpressing glucose transporter protein and were able to efficiently label  $^{68}\text{Ga}$  (labeling efficiency  $\geq 85\%$ ). After CpG loading, the formed DG-Au DENPs/CpG polyplexes can be used for dual-mode tumor PET/CT imaging and immunotherapy by effectively maturing dendritic cells to induce T-cell-based antitumor immune response. The developed DG-Au DENPs/CpG polyplexes show more sensitive imaging and better tumor suppression efficacy than DG-free polyplexes.<sup>43</sup>

## 4. Conclusion and outlook

This review summarizes recent advances in the use of PAMAM dendrimer-based nanoplatfoms for CT contrast agents in recent years. Due to their unique structural and physicochemical properties, dendrimer-loaded I-containing contrast agents can overcome the shortcomings of traditional small-molecule I-based contrast agents. Since Au has a higher atomic number than I, dendrimer-entrapped or -stabilized Au NPs or Au DSNSs have better X-ray attenuation coefficients and therefore have better imaging sensitivity than I-based CT contrast agents. Further, the integration of multiple contrast agents such as  $\text{Fe}_3\text{O}_4$  NPs, Mn and Gd ions, radioisotopes and fluorescent molecules using dendrimer nanoplatfoms allows for dual-mode or multimode imaging. Lastly, physically encapsulating, adsorbing or covalently binding drugs or genes in the cavities or on the surface of the PAMAM dendrimers can render the platfoms with integrated application of tumor diagnosis and treatment.

Although the use of PAMAM dendrimer-based nanoplatfoms for tumor CT imaging and theranostics has been extensively studied, more exploration is still needed in both laboratory studies and translation to the clinic. First, for laboratory research, with the progress of tumor biology and nanotechnology, the design of smarter, more specific, and higher-sensitivity contrast agents based on dendrimer nanocomplexes is still attractive, such as developing new contrast components to improve the imaging quality and exploring new targeted delivery methods to further reduce side effects. Second, for clinical translation, the use of dendrimer nanoplatfoms for CT imaging is still in its infancy. It is hoped that theoreticians, experimentalists and clinicians will explore the main challenges and opportunities from a systems science perspective. For example, based on the existing laboratory progress, we can design the optimal composition and structure of the PAMAM dendrimer-based nanoplatfom, explore the function and properties of the material itself, and evaluate its impact and diagnostic and therapeutic functions at the levels of gene–cell–tissue–small animal model–large animal model–human, and finally achieve precision medicine and significantly improve the treatment outcomes. Finally, we expect that the PAMAM dendrimer-based nanoplatfoms and nanomedicines will be translated for the benefit of patients.

## Author contributions

Tianyu Huang: software, writing – original draft. Gaoming Li: software, writing – original draft. Yunqi Guo: writing – review & editing. Guixiang Zhang: funding acquisition, writing – review & editing. Dzmitry Shchabin: writing – review & editing. Xiangyang Shi: supervision, resources, funding acquisition, project administration, writing – review & editing. Mingwu Shen: supervision, resources, funding acquisition, project administration, writing – review & editing.

## Conflicts of interest

The authors declare no conflict of interest.

## Acknowledgements

This study was financially supported by the National Key R&D Program (2022YFE0196900), the Science and Technology Commission of Shanghai Municipality (20520710300, 21490711500, and 20DZ2254900), the Shanghai Education Commission through the Shanghai Leading Talents Program, and the Fundamental Research Funds for the Central Universities (2232021A-03).

## References

- 1 R. L. Siegel, K. D. Miller, H. E. Fuchs and A. Jemal, *Ca-Cancer J. Clin.*, 2022, **72**, 7–33.
- 2 L. T. Wang, J. L. Wang, H. W. Liu, Y. Ge, Y. Y. Li and Q. X. Xu, *J. Chin. Pharm. Sci.*, 2017, **48**, 635–645.
- 3 X. X. Wang, C. Kong, W. Z. Xu, S. Yang, D. Shi, J. Y. Zhang, M. L. Du, S. W. Wang, Y. K. Bai, T. Zhang, Z. Chen, Z. F. Ma, J. Wang, G. C. Dong, M. T. Sun, R. Yin and F. Chen, *Thorac. Cancer*, 2019, **10**, 1904–1912.
- 4 A. C. Tsili, C. Naka and M. I. Argyropoulou, *Acta Radiol.*, 2021, **62**, 1696–1706.
- 5 M. Longmire, P. L. Choyke and H. Kobayashi, *Curr. Top. Med. Chem.*, 2008, **8**, 1180–1186.
- 6 Z. Qiao and X. Y. Shi, *Prog. Polym. Sci.*, 2015, **44**, 1–27.
- 7 Y. Fan, W. J. Sun and X. Y. Shi, *Small Methods*, 2017, **1**, 1700224.
- 8 D. Li, S. H. Wen and X. Y. Shi, *Wiley Interdiscip. Rev.: Nanomed. Nanobiotechnol.*, 2015, **7**, 678–690.
- 9 S. Suty, V. Oravczova, Z. Garaiova, V. Subjakova, M. Ionov, D. Shcharbin, Z. Simonikova, P. Bartek, M. Zvarik, X. Y. Shi, S. Mignani, J. P. Majoral, M. Bryszewska, T. Hianik and I. Waczulikova, *Biomedicines*, 2021, **9**, 1672.
- 10 F. Shi, C. Peng, Y. Yang, Y. Sha, X. Y. Shi and H. T. Wu, *Colloids Surf., A*, 2016, **497**, 194–204.
- 11 R. N. Liu, H. H. Guo, Z. J. Ouyang, Y. Fan, X. Y. Cao, J. D. Xia, X. Y. Shi and R. Guo, *ACS Appl. Bio Mater.*, 2021, **4**, 1803–1812.
- 12 J. J. Liu, G. M. Li, H. H. Guo, C. Ni, Y. Gao, X. Y. Cao, J. D. Xia, X. Y. Shi and R. Guo, *ACS Appl. Mater. Interfaces*, 2023, **15**, 12809–12821.



- 13 W. Y. He, K. L. Ai and L. H. Lu, *Sci. China: Chem.*, 2015, **58**, 753–760.
- 14 N. Lee, S. H. Choi and T. Hyeon, *Adv. Mater.*, 2013, **25**, 2641–2660.
- 15 R. Guo, H. Wang, C. Peng, M. W. Shen, L. F. Zheng, G. X. Zhang and X. Y. Shi, *J. Mater. Chem.*, 2011, **21**, 5120–5127.
- 16 C. Peng, K. Li, X. Y. Cao, T. T. Xiao, W. X. Hou, L. F. Zheng, R. Guo, M. W. Shen, G. X. Zhang and X. Y. Shi, *Nanoscale*, 2012, **4**, 6768–6778.
- 17 T. T. Xiao, J. B. Qin, C. Peng, R. Guo, X. W. Lu and X. Y. Shi, *Langmuir*, 2020, **36**, 3096–3103.
- 18 S. You, H. Y. Jung, C. Lee, Y. H. Choe, J. Y. Heo, G. T. Gang, S. K. Byun, W. K. Kim, C. H. Lee, D. E. Kim, Y. I. Kim and Y. Kim, *J. Controlled Release*, 2016, **226**, 258–267.
- 19 P. Mohammadzadeh, M. Shafiee Ardestani, S. Mortazavi-Derazkola, A. Bitarafan-Rajabi and S. M. Ghoreishi, *IET Nanobiotechnol.*, 2019, **13**, 560–564.
- 20 Z. J. Xiong, Y. Wang, J. Y. Zhu, X. Li, Y. He, J. Qu, M. W. Shen, J. D. Xia and X. Y. Shi, *Nanoscale*, 2017, **9**, 12295–12301.
- 21 Y. F. Zhang, Y. Y. Luo, X. L. Wu, L. Q. Yang, D. D. Cui, C. Z. Wei and W. Z. Wang, *Sci. Adv. Mater.*, 2021, **13**, 1674–1684.
- 22 X. Y. Xu, K. Liu, Y. Wang, C. C. Zhang, M. H. Shi, P. Wang, L. H. Shen, J. D. Xia, L. Ye, X. Y. Shi and M. W. Shen, *J. Mater. Chem. B*, 2019, **7**, 3639–3643.
- 23 J. Y. Liu, Z. J. Xiong, J. L. Zhang, C. Peng, B. Klajnert-Maculewicz, M. W. Shen and X. Y. Shi, *ACS Appl. Mater. Interfaces*, 2019, **11**, 15212–15221.
- 24 J. S. Chen, J. W. Chen, S. Bhattacharjee, Z. Y. Cao, H. Wang, S. D. Swanson, H. Zong, J. R. Baker and S. H. Wang, *J. Nanobiotechnol.*, 2020, **18**, 135.
- 25 Y. M. Zhang, R. N. Pei and T. Luo, *Sci. Adv. Mater.*, 2021, **13**, 1364–1373.
- 26 R. Wang, Y. Luo, S. Yang, J. Lin, D. Gao, Y. Zhao, J. Liu, X. Shi and X. Wang, *Sci. Rep.*, 2016, **6**, 33844.
- 27 X. Xu, T. T. Xiao, C. C. Zhang, Z. Q. Wang, G. M. Li, J. W. Chen, Z. J. Ouyang, H. Wang, X. Y. Shi and M. W. Shen, *Biomacromolecules*, 2023, **24**, 967–976.
- 28 Y. C. Peng, X. M. Wang, Y. Wang, Y. Gao, R. Guo, X. Y. Shi and X. Y. Cao, *Pharmaceutics*, 2021, **13**, 995.
- 29 M. X. Chen, O. Betzer, Y. Fan, Y. Gao, M. W. Shen, T. Sadan, R. Popovtzer and X. Y. Shi, *Biomacromolecules*, 2020, **21**, 1587–1595.
- 30 X. Li, Z. G. Xiong, X. Y. Xu, Y. Luo, C. Peng, M. W. Shen and X. Y. Shi, *ACS Appl. Mater. Interfaces*, 2016, **8**, 19883–19891.
- 31 X. Y. Xu, L. Z. Zhao, X. Li, P. Wang, J. H. Zhao, X. Y. Shi and M. W. Shen, *Biomater. Sci.*, 2017, **5**, 2393–2397.
- 32 Y. Xing, J. Y. Zhu, L. Z. Zhao, Z. J. Xiong, Y. J. Li, S. Wu, G. Chand, X. Y. Shi and J. H. Zhao, *Drug Delivery*, 2018, **25**, 1384–1393.
- 33 Y. J. Li, L. Z. Zhao, X. Y. Xu, N. Sun, W. L. Qiao, Y. Xing, M. W. Shen, M. L. Zhu, X. Y. Shi and J. H. Zhao, *J. Biomed. Nanotechnol.*, 2019, **15**, 1201–1212.
- 34 P. Wei, J. W. Chen, Y. Hu, X. Li, H. Wang, M. W. Shen and X. Y. Shi, *Adv. Healthcare Mater.*, 2016, **5**, 3203–3213.
- 35 S. Y. Lu, X. Li, J. L. Zhang, C. Peng, M. W. Shen and X. Y. Shi, *Adv. Sci.*, 2018, **5**, 1801612.
- 36 M. Alibolandi, F. Hoseini, M. Mohammadi, P. Ramezani, E. Einafshar, S. M. Taghdisi, M. Ramezani and K. Abnous, *Int. J. Pharm.*, 2018, **549**, 67–75.
- 37 J. Y. Zhu, G. Wang, C. S. Alves, H. Tomas, Z. J. Long, M. W. Shen, J. Rodrigues and X. Y. Shi, *Langmuir*, 2018, **34**, 12428–12435.
- 38 Y. Fan, W. Z. Tu, M. W. Shen, X. M. Chen, Y. S. Ning, J. J. Li, T. F. Chen, H. Wang, F. F. Yin, Y. Liu and X. Y. Shi, *Adv. Funct. Mater.*, 2020, **30**, 1909285.
- 39 S. Yamashita, H. Katsumi, E. Shimizu, Y. Nakao, A. Yoshioka, M. Fukui, H. Kimura, T. Sakane and A. Yamamoto, *Eur. J. Pharm. Biopharm.*, 2020, **157**, 85–96.
- 40 Y. Gao, Z. J. Ouyang, C. Yang, C. Song, C. J. Jiang, S. L. Song, M. G. Shen and X. Y. Shi, *Adv. Healthcare Mater.*, 2021, **10**, 2100833.
- 41 L. L. Ye, Y. M. Chen, J. Z. Mao, X. T. Lei, Q. Yang and C. H. Cui, *J. Exp. Clin. Cancer Res.*, 2021, **40**, 303.
- 42 F. F. Yin, Y. Fan, L. J. Xu, F. Yin, M. J. He, T. T. Xiao, X. Y. Shi and H. Wang, *Chem. Eng. J.*, 2021, **417**, 129273.
- 43 C. Li, L. Z. Zhao, L. Jia, Z. J. Ouyang, Y. Gao, R. Guo, S. L. Song, X. Y. Shi and X. Y. Cao, *J. Mater. Chem. B*, 2022, **10**, 3648–3656.
- 44 S. Chauhan, K. Patel, P. Jain, A. K. Jangid, S. Patel, K. Medicherla, K. Limbad, C. Mehta and H. Kulhari, *Drug Dev. Ind. Pharm.*, 2022, **48**, 333–342.
- 45 Y. Hu, J. C. Li, M. W. Shen and X. Y. Shi, *Chin. Phys. B*, 2014, **23**, 078704.
- 46 S. R. Barman, A. Nain, S. Jain, N. Punjabi, S. Mukherji and J. Satija, *J. Mater. Chem. B*, 2018, **6**, 2368–2384.
- 47 Q. H. Sun, X. R. Sun, X. P. Ma, Z. X. Zhou, E. L. Jin, B. Zhang, Y. Q. Shen, E. A. Van Kirk, W. J. Murdoch, J. R. Lott, T. P. Lodge, M. Radosz and Y. L. Zhao, *Adv. Mater.*, 2014, **26**, 7615–7621.
- 48 L. Jia, X. Li, H. Liu, J. D. Xia, X. Y. Shi and M. W. Shen, *Nano Today*, 2021, **36**, 101022.
- 49 Y. Q. Guo, Y. Fan, G. M. Li, Z. Q. Wang, X. Y. Shi and M. W. Shen, *ACS Appl. Mater. Interfaces*, 2021, **13**, 55815–55826.
- 50 T. T. Xiao, W. Hu, Y. Fan, M. W. Shen and X. Y. Shi, *Theranostics*, 2021, **11**, 7057–7071.
- 51 T. T. Xiao, M. J. He, F. Xu, Y. Fan, B. Y. Jia, M. W. Shen, H. Wang and X. Y. Shi, *ACS Nano*, 2021, **15**, 20377–20390.
- 52 J. W. Chen, Y. Q. Sun, Q. Chen, L. Wang, S. H. Wang, Y. Tang, X. Y. Shi and H. Wang, *Nanoscale*, 2016, **8**, 13568–13573.
- 53 X. Bi, X. Shi, I. J. Majoros, R. Shukla and J. R. Baker, *J. Comput. Theor. Nanosci.*, 2007, **4**, 1179–1187.
- 54 H. Liu, J. Y. Zhu, J. L. Zhao, G. X. Zhang and X. Y. Shi, *J. Controlled Release*, 2013, **172**, E37–E38.
- 55 L. F. Zheng, J. Y. Zhu, M. W. Shen, X. S. Chen, J. R. Baker, S. H. Wang, G. X. Zhang and X. Y. Shi, *MedChemComm*, 2013, **4**, 1001–1005.
- 56 D. C. Xie and K. P. Xie, *Genes Dis.*, 2015, **2**, 133–143.



- 57 J. X. Ding, J. J. Chen, L. Q. Gao, Z. Y. Jiang, Y. Zhang, M. Q. Li, Q. C. Xiao, S. S. Lee and X. S. Chen, *Nano Today*, 2019, **29**, 100800.
- 58 P. P. Provenzano, C. Cuevas, A. E. Chang, V. K. Goel, D. D. Von Hoff and S. R. Hingorani, *Cancer Cell*, 2012, **21**, 418–429.
- 59 M. E. Keir, M. J. Butte, G. J. Freeman and A. H. Sharpel, *Annu. Rev. Immunol.*, 2008, **26**, 677–704.
- 60 X. Xue, J. Li, Y. Fan, M. W. Shen and X. Y. Shi, *Sci. China Mater.*, 2021, **64**, 2045–2055.

